



# Thickness effect on the fracture and delamination of titanium films



M.J. Cordill <sup>a,\*</sup>, A.A. Taylor <sup>b,c</sup>

<sup>a</sup> Erich Schmid Institute of Materials Science, Austrian Academy of Science and the Department of Materials Physics, Montanuniversität Leoben, Jahnstrasse 12, 8700 Leoben, Austria

<sup>b</sup> Physics Department, Durham University, Durham DH1 3LE, UK

<sup>c</sup> Laboratory for Mechanics and Nanostructures, Empa, Swiss Federal Laboratories for Materials Testing and Research, Feuerwerkerstrasse 39, CH-3602 Thun, Switzerland

## ARTICLE INFO

### Article history:

Received 13 December 2014

Received in revised form 6 May 2015

Accepted 14 May 2015

Available online 23 May 2015

### Keywords:

Transmission electron microscopy

Fragmentation testing

Coating adhesion

Microstructure–property relationships

## ABSTRACT

Titanium adhesion layers are a common component of many coated products; they play a particularly important role in promoting the adhesion of Cu and Au conduction lines to polymer substrates for flexible electronic circuitry. In this work a full microstructural and mechanical characterization is performed on Ti layers of three different thicknesses—8, 12 and 50 nm—deposited onto polyimide. Observed differences in the mechanical behavior of the coatings were found to relate to the changing chemistry and grain size of the coatings. In particular, the observation, using transmission electron microscopy, that the two thinner coatings were comprised of 50% or less metallic Ti illustrates the potential pitfalls of altering something so simple as the coating thickness.

© 2015 Elsevier B.V. All rights reserved.

## 1. Introduction

Thin film mechanical behavior can be difficult to measure, especially when the film thickness is less than 100 nm. However, the mechanical as well as interfacial behavior of the thin films deposited onto polymer substrates is important to understand for applications in flexible electronics, sensors, coatings, and bio applications [1,2]. The mechanical and interfacial behavior will depend on the resulting film microstructure and interface structure. Usually, the mechanical response, fracture strain or yield stress, increases with decreasing film thickness. This size effect could be due to the film thickness decrease, but also the decrease in grain size due to the reduced thickness. On the other hand, the interfacial behavior, or adhesion, should not change with the film thickness as long as the same interface is failing.

A method that can be used to determine the mechanical and interfacial properties of metal films on polymer substrates is fragmentation testing [3–6]. This technique strains the film–substrate system in uniaxial tension to induce film cracking (fracture) and at higher strains (>8%) film delamination can occur between the crack fragments [4–6]. When fragmentation testing is performed in-situ, with optical light microscopy, scanning electron microscopy (SEM), or 4-point-probe (4PP) resistance measurements [6–9], the initial fracture strain,  $\varepsilon_f$ , can be ascertained. The minimum crack spacing at saturation,  $\lambda_{\min}$ , and

the initial fracture strain can be used with the shear lag model [4,10] to calculate the interfacial shear stress,  $\tau_{IFSS}$  (Eq. (1)), with

$$\tau_{IFSS} = \frac{\pi h \sigma_f}{2 \lambda_{\min}}, \quad (1)$$

where  $h$  is the film thickness, and  $\sigma_f$  is the fracture stress ( $\sigma_f = E\varepsilon_f$ ). Recent work by the authors [6,11] has demonstrated that caution must be exercised in the application of shear lag type models to metallic and ceramic coatings on polymer substrates. This caution is required because the large difference in elastic moduli between film and substrate, sometimes two orders of magnitude difference, can cause bending of the film and a rather more complicated stress state at the interface than that assumed by shear lag. The applicability of such models should be ascertained through some basic analysis of the crack spacing distribution once saturation has been reached. A key prediction of the shear lag model is that at crack saturation the widest spacing between cracks is equal to twice the narrowest. Variations in film thickness and in film fracture strength mean that this is rarely the case. However, Taylor et al. [11] demonstrated that a comparison of each crack spacing with its two neighbors can greatly reduce the effects of these variations and hence the measurement of such neighbor ratios is recommended when applying shear lag mechanics.

Utilizing the height,  $\delta$ , and half buckle width,  $b$ , of the delaminated regions (called buckles) and the thermo-mechanical model of Cordill et al. [12] the adhesion energy of a metal–polymer interface can be measured. The model takes into account the strain energy between the resulting buckles, the debonding energy of the interface, and the strain

\* Corresponding author. Tel.: +43 3842804112; fax: +43 3842804116.  
E-mail address: [megan.cordill@oeaw.ac.at](mailto:megan.cordill@oeaw.ac.at) (M.J. Cordill).

energy of the buckles. It has been shown that the method to brittle films [12–14] or multilayer films that behave in a brittle manner [15–18].

In the various studies of thin film fracture behavior and adhesion measured with fragmentation, knowledge of the film microstructure and interface structure is often lacking [4,5,19–21]. The assumption that the grain size is the same as the film thickness does not always hold true. And, as demonstrated by measurements in ultra-fine grained or nanocrystalline metals, the fracture behavior changes with grain size, as does the propagation path of the cracks [22,23]. Intimate knowledge of the interface structure is also necessary to understand the adhesion energy and how the interface fails, as previously shown by Taylor et al. [13]. Not only the interface structure but the interface chemistry will also influence the adhesion energy.

Presented here is an in-depth study of the mechanical behavior (fracture and adhesion) of thin Ti films (8–50 nm) on polyimide (PI) with respect to the microstructure and interface structure. Ex-situ and in-situ 4 point probe (4PP) fragmentation testing are employed to study the fracture and adhesion while high resolution transmission electron microscopy (HRTEM) and scanning TEM (STEM) is used to evaluate the resulting film grain size and interface structure.

## 2. Experimental

The Ti films were deposited with electron beam evaporation onto cleaned UPILEX brand 50  $\mu\text{m}$  thick polyimide (PI). The PI film was first cleaned by soaking in a 10% aqueous solution of RBS 50 (a laboratory cleaning concentrate with high pH). After soaking for 24 h at room temperature the substrates were rinsed with deionized water and a 1 MHz ultrasonic cleaning process. The Ti films were deposited in a Balzers BAK 550 evaporation machine with the vacuum at  $2.10 \times 10^{-7}$  mbar and using a deposition rate of 0.2 nm/s for the nominal 8 nm and 12 nm thick films and 0.5 nm/s for the nominally 50 nm thick film. These ultra-thin thicknesses represent typical adhesion layers for flexible electronics applications. The residual stresses in the films were not able to be measured by other techniques such as the  $\sin^2 \Psi$  method with X-ray diffraction. After deposition the samples were flat and did not exhibit any macroscopic bending typical of films on polymer substrates with high residual stresses.

Cross-sectional and plan view transmission electron microscopy (TEM, JEOL 2100F) was used to examine the film microstructure and interface structure. Cross-sectional TEM samples were made by focused ion beam (FIB, FEI Helios Nanolab) lift-out [24]. A 1  $\mu\text{m}$  thick layer of Pt was deposited onto the area of interest with the electron beam prior to lift-out in order to prevent ion-beam damage to the film. The samples were milled from 3000 nm down to around 200 nm thickness by parallel milling with the beam acceleration being decreased from 15 kV down to 5 kV. Final polishing of the samples was then carried out at 2 kV and 1 kV at a  $7^\circ$  incline to the sample surface; this reduced the samples to around 50 nm thickness in the areas examined. Plan view samples were prepared by straining the film–substrate system and mechanically removing the film from the substrate [25] (samples strained to 20%). These samples were principally used to obtain grain size statistics for the films.

To study the fracture and adhesion properties of the different film thicknesses, fragmentation testing was employed [3,6–9]. Two straining stages were utilized to strain in uni-axial tension to cause fracture and delamination of the films. For the ex-situ experiments a Kammerath & Weiss (Germany) small scale straining device was employed to strain the films to 15–17% engineering strain. In-situ fragmentation tests were performed on an MTS Tytron® with in-situ 4PP resistance measurements. The electrical resistance measurements were made with the 4-point-probes incorporated into the grips [8]. In-situ 4PP experiments were performed in order to obtain a more exact measure of the fracture strain since the resistance of the film will increase dramatically with the introduction of a single crack and deviate from the theoretical

behavior as described by a volume conservation [8,9]. The samples tested by in-situ 4PP were strained to 20%.

Post-mortem experimental examination of all strained samples with SEM and atomic force microscopy (AFM) was performed to characterize the cracking and buckling behavior of the different film thicknesses. From the SEM images the crack spacing,  $\lambda$ , was measured using Image J [26]. Using the minimum saturation crack spacing ( $>10\%$  strain) and the initial fracture strain, the interfacial shear stress,  $\tau_{IFSS}$ , was calculated with Eq. (1) following neighbor ratio verification that the shear lag model is valid. In order to determine the crack spacing distribution for the films, spacings were measured from four SEM micrographs taken across the entire length of a sample strained to at least 15%, which is well within the saturation regime for these films [13]. Then the ten shortest (minimum) measured crack spacings were averaged to find the average,  $\lambda_{\text{min}}$ , used in determining  $\tau_{IFSS}$ . Neighbor ratios were determined for the three coating thicknesses following Ref. [11]. Because brittle cracking via through thickness cracks occurred for all film thicknesses, strain recovery was not considered to be an issue for the crack spacing measurements.

AFM was used to measure the buckle dimensions in order to calculate the adhesion energy of the Ti–PI interface using the model from Cordill et al. [12]. The ends of 20–30 partial buckles on each film were measured to evaluate the adhesion energy. Partial buckles, those which have not traveled across the crack fragment, have been shown to be the ideal geometry and size to determine the adhesion energy using fragmentation induced delamination [12–14,17]. An example of the buckle measurement is shown in Fig. 1 for the 12 nm film. All buckles were measured after approximately 15% strain. Again, strain recovery was not considered to be an influencing factor for the AFM buckle measurements of these brittle films. For more ductile or poorly adhering films, strain recovery should be taken into account.

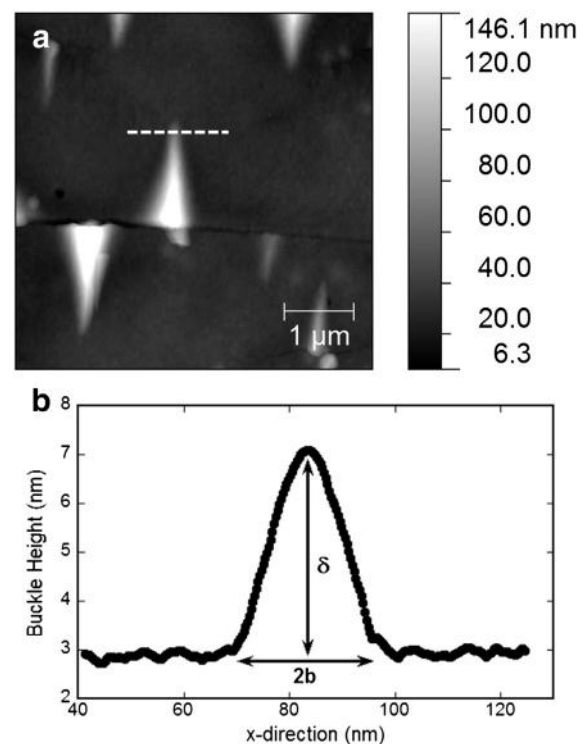


**Fig. 1.** (a) AFM height image of cracked and buckled 12 nm Ti film after 15% strain (straining direction vertical). (b) Corresponding height profile of the dashed line in (a) of the measured buckle. Using the height profile, the buckle height,  $\delta$ , and buckle width,  $2b$ , can be measured.

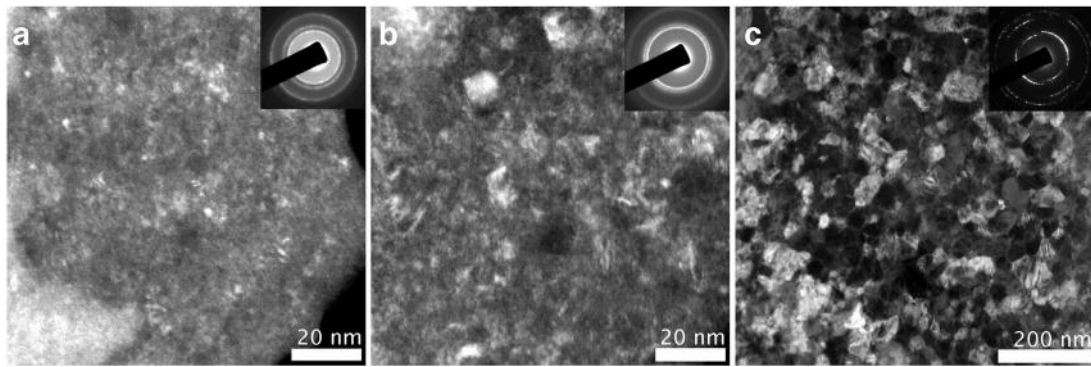


**Fig. 2.** Plan-view DF-STEM micrographs of the three Ti films (a) 8 nm, (b) 12 nm, and (c) 50 nm. Note the change in scale bar in (c). The corresponding diffraction patterns for the images are included as inserts.

### 3. Results and discussion

The microstructures for the three films are shown in the plan view dark field scanning TEM (DF-STEM) micrographs in Fig. 2. It can be seen that the grain size of the films decreases with film thickness, as is expected, from 32 nm in the thickest film to around 1.4 nm in the thinnest; a summary of the measured grain sizes is presented in Table 1. Cross-sectional TEM of the three film thicknesses are presented in Fig. 3. It is important to note from these micrographs that the three different thickness coatings are all comprised of a  $\text{TiO}_x$  surface oxide, a Ti layer and a Ti–PI interlayer [13]. The thickness of the  $\text{TiO}_x$  layer and the Ti–PI interlayer is observed to be constant between the samples while the thickness of the Ti layer scales with film thickness (Table 1). The discovery of a Ti–PI interlayer between the pure Ti film and the PI substrate is not surprising. Some thin film adhesion studies have assessed the chemistry of the film and substrate after a peel test to determine if film residue is left on the substrate after mechanical removal [27,28]. Other more in-depth investigations use in-situ X-ray photoelectron spectroscopy (XPS) experiments [29–34] or in-situ Auger electron spectroscopy (AES) [35] to reveal the bonding nature of metals to polymers over a few monolayers. The main finding of

these investigations has been that during the first few monolayers of deposition, a compound of the depositing film, carbon, and oxygen forms first. The desired film grows without significant additional elements being incorporated after the reaction layer reaches a critical thickness. These few atomic layers help to ensure good bonding between the metal and polymer.

When the three films are subjected to fragmentation testing the fracture behavior changes with increasing film thickness. As shown in Fig. 4, the 8 nm film fractures with straight cracks and the 50 nm with zig-zag cracks. The 12 nm film fails through both straight and zig-zag cracks and appears to be a transition thickness between the two cracking morphologies. The average saturation crack spacing increases with increasing film thickness, as expected (Table 2). In-situ 4PP straining experiments measured fracture strains of about 4.5% for the three film thicknesses (Table 2). If the films contained a large residual stress, they would macroscopically bend and increase the initial fracture strain (compressive residual stress) or decrease the initial fracture stress (tensile residual stress). Before the fracture stresses were calculated from the fracture strains, the crack spacing and neighbor ratio distributions were generated for the three film thicknesses (Fig. 5a). The range of the crack spacing distributions was found to be in excess of the factor

**Table 1**

Average film thickness and grain size of the studied films.

Nominal film	Ave. grain	Total film	Interlayer film	Ti film	TiO <sub>x</sub> film
Thickness (nm)	Size (nm)	Thickness (nm)	Thickness (nm)	Thickness (nm)	Thickness (nm)
8	1.4 ± 0.4	12 ± 2	4.5 ± 1	4.5 ± 1	3 ± 1
12	5.5 ± 1.6	17 ± 3	5 ± 1	9 ± 1	3 ± 1
50	32 ± 8	52 ± 4	5 ± 1	44 ± 2	3.5 ± 1

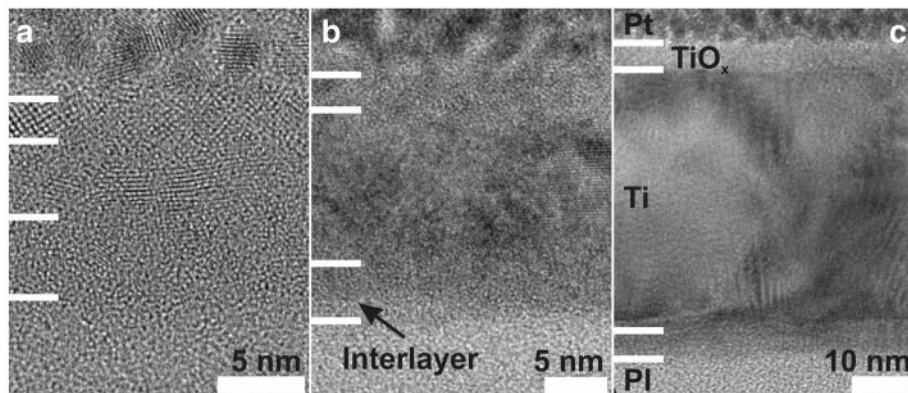


**Fig. 3.** HRTEM cross-section micrographs of the three Ti films. The thicknesses of the Ti–PI interlayer and the  $\text{TiO}_x$  surface oxide do not vary with film thickness. Note the change in scale bar in (c).

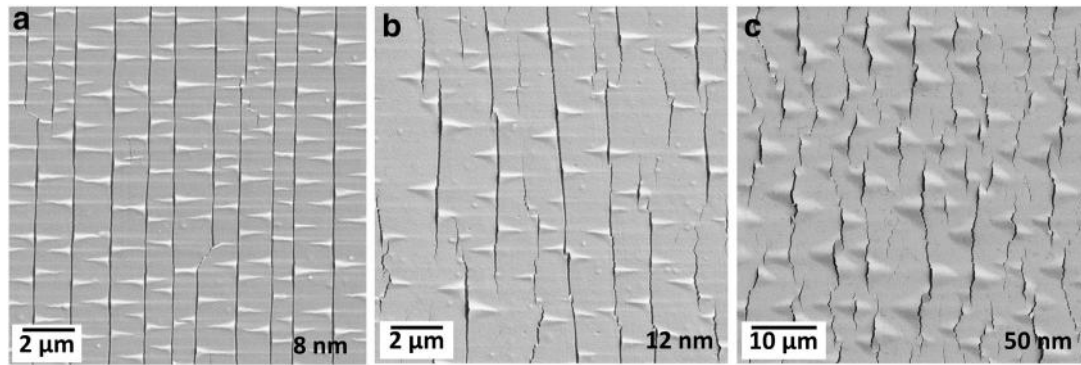


**Fig. 4.** SEM micrographs of Ti films strained approximately 15% (a) 8 nm with straight cracks and buckles, (b) 12 nm with straight and zig-zag cracks as well as triangular buckles, and (c) zig-zag cracks with large triangular buckles. Note the change in scale bar in (c).

**Table 2**

Summary of the mechanical behavior results. An elastic modulus for Ti of 116 GPa was used for the calculation of the interfacial shear stress.

Nominal film Thickness (nm)	Ave. saturation crack Spacing (μm)	% fracture Strain, $\epsilon_f$	Calc. fracture Stress (GPa)	Min. crack Spacing (μm)	Calc. $\tau_{IFSS}$ (MPa)	Adhesion energy $r$ ( $Jm^{-2}$ )
8	$1.1 \pm 0.3$	$3.8 \pm 0.14$	$4.4 \pm 0.7$	$0.6 \pm 0.07$	$139 \pm 62$	$4.7 \pm 1.3$
12	$2.3 \pm 0.6$	$4.8 \pm 0.2$	$5.6 \pm 1.3$	$1.3 \pm 0.12$	$114 \pm 57$	$5 \pm 1.7$
50	$3.6 \pm 1.2$	4.9	5.70	$3.1 \pm 0.22$	$150 \pm 22$	$4.1 \pm 0.8$

two predicted by shear lag theory for all the investigated coatings (Table 2). However, the neighbor ratio data (Fig. 5b) demonstrates that the majority of the distribution lies between 1 and 2, i.e. most of the neighboring crack fragments do not exceed the factor of two, and hence shear lag can be applied to these samples. Examples of neighbor ratio distributions, and corresponding micrographs, from coatings where the ratio regularly exceeds 2 can be found in reference [6].

Using the fragmentation results, the fracture stress and minimum crack spacing; the interfacial shear stress of the investigated Ti films can be calculated using Eq. (1). A minimum in the  $\tau_{IFSS}$  is observed for the 12 nm film while the values for the 8 nm and 50 nm film thicknesses are similar; this is an indication of a transition thickness or grain size for two different thin film fracture behaviors. The calculated values using the shear lag theory are presented in Table 2 for all film thicknesses. It can be inferred from the microstructural and mechanical results that a combination of two factors is affecting the fracture behavior of the films. The first is the reduction in the total amount of Ti. This causes the brittle behavior of the interlayer and  $TiO_x$  to dominate the fracture

behavior by decreasing any Ti-mediated toughening via plastic deformation and crack deflection. The second factor is the change in grain size. The larger grains of the 50 nm film allow for easier nucleation and glide of dislocations while also causing greater deflections to cracks that propagate via grain boundaries. The fact that both straight and zig-zag cracks are observed in the 12 nm film provides further evidence that this is a critical thickness for the activation of toughening mechanisms.

Investigating the mechanical properties of ultra thin films, particularly those deposited on polymer substrates, is complicated by the difficulty in determining the elastic constants of the film [36,37]. The necessity for extensive research in the area of thin films is largely driven by the unusual physical properties of materials at these dimensions [38, 39], this does however complicate any calculations where these parameters could be changing between the studied samples. In the present case, it has been assumed in the calculation of the interfacial shear stress that the elastic modulus of the  $TiO_x/Ti/Ti-PI$  multilayer is the same for all three thicknesses, 116 GPa. It is unlikely that the  $TiO_x$  surface oxide and  $Ti-PI$  interlayer have the same elastic constants as Ti. In order to

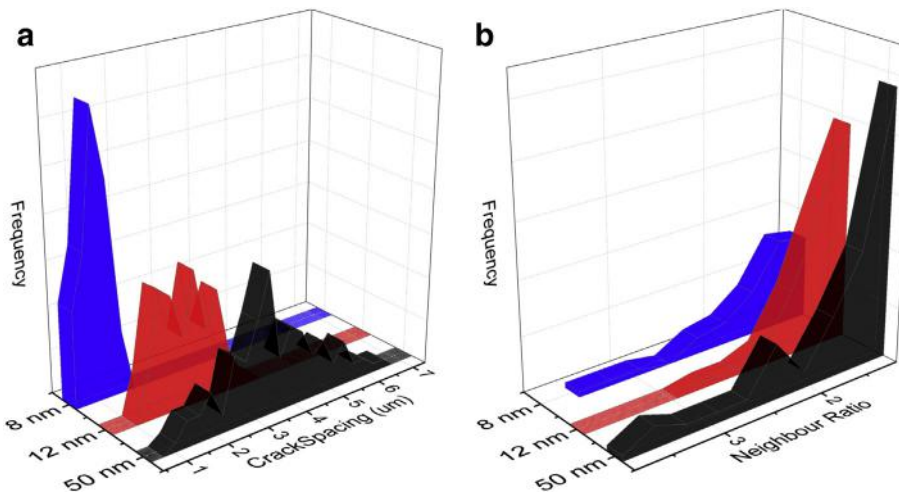


**Fig. 5.** (a) Crack spacing distributions and (b) neighbor ratio distributions for the three Ti films. The majority of neighbor ratios lying between 1 and 2 in (b) indicates that the shear lag model can be applied to these coatings.

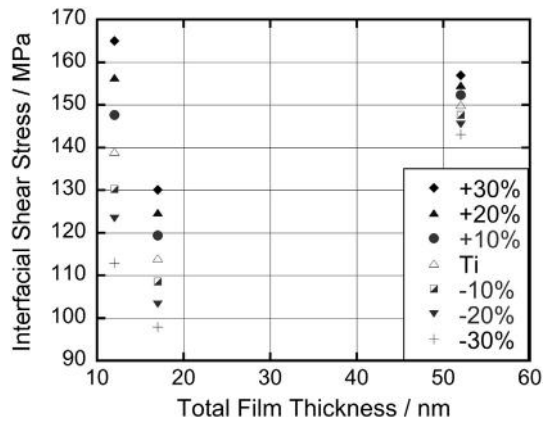


**Fig. 6.** The calculated  $\tau_{\text{IFSS}}$  is plotted using stiffnesses for the  $\text{TiO}_x$  and Ti–PI layers of +30% to –30% with respect to Ti. Determining the real elastic properties of these layers would be very challenging but this analysis demonstrates that the exact Young's modulus values do not affect the overall trend.

justify the conclusions drawn from the mechanical data, a simple comparison of the calculated  $\tau_{\text{IFSS}}$  for the different film thicknesses is presented in Fig. 6 where the average modulus of the combined non-metallic layers is varied by +30% to –30% with respect to metallic Ti. It can be seen from Fig. 6 that while the absolute values of  $\tau_{\text{IFSS}}$  change more for the thinner coatings, where a greater fraction of non-metallic Ti is present, the observed trend remains the same.

Not only does the cracking behavior change with film thickness, but also the buckling behavior. The 8 nm buckles are narrow and straight and the 12 nm and 50 nm thick films have triangular shaped buckles. In order to measure the adhesion of the interfaces, the buckle dimensions,  $\delta$  and  $b$ , are plotted as  $(\delta/h)^{1/2}$  versus  $(b/h)$ . Then the lower bound of the data points can be described by Eq. (2) and varying the fitting parameter,  $\alpha_A$

$$(\delta/h)^{1/2} = (2\alpha_A)^{1/4} (b/h) \left[ 1 + \sqrt{1 + (3/4)\alpha_A (b/h)^4} \right]^{-1/4} \quad (2)$$

It has been shown [12–17] that it is best to use a minimum  $\alpha_A$  value as this best corresponds to uncracked buckles with a more regular and curved cross-section. Using the  $\alpha_A$  parameter that best fits the lower bound of the data, the adhesion energy,  $\Gamma$ , is calculated using

$$\Gamma = \frac{hE'\alpha_A}{0.657} \quad (3)$$

In Eq. (3),  $h$  is the film thickness and  $E'$  is the modified elastic modulus. The modified elastic modulus takes into account the elastic

modulus,  $E$  and Poisson's ratio,  $\nu$ , of the titanium film as  $E' = E / (1 - \nu^2)$ . For Ti an  $E = 116$  GPa and  $\nu = 0.32$  were utilized. From the buckle measurements, the adhesion energies were calculated using three different  $\alpha_A$  values ( $4 \times 10^{-4}$ ,  $1.5 \times 10^{-3}$ , and  $2.5 \times 10^{-3}$ , respectively for the 8, 12, and 50 nm films) as shown in Fig. 7. In Fig. 7, each point is one buckle measurements and only a lower bound fit of the data with Eq. (2) with the appropriate  $\alpha_A$  value are needed for the adhesion measurement. Examination of the polymer substrate surface beneath buckled areas of film with cross-sectional TEM determined that delamination occurs at the Ti–PI interface, therefore the total thickness of the three layers is used in the adhesion calculations. The adhesion energies are relatively constant as a function of the film thickness ( $4.5 \text{ Jm}^{-2}$ ) which is expected because the same interface with the same interface structure failed in all cases. The calculated adhesion energies can be found in Table 2 and compare well with similar metal–polymer systems [12–17]. It should also be noted that the change in crack path or buckle shape did not affect the measured adhesion energies as the film thickness was increased.

#### 4. Summary

In this study, the microstructure and mechanical behavior of thin Ti films (nominally 8–50 nm) on PI were examined using TEM and fragmentation testing. The use of multiple characterization methods was necessary to understand the different behavior of the coatings as a function of film thickness. The TEM grain size assessment found that the grain sizes were not the same as the nominal thickness, rather much smaller. With cross-sectional TEM it was observed that the films were actually made of three different layers, a Ti–PI interlayer, Ti layer, and a  $\text{TiO}_x$  surface oxide, with the Ti–PI and  $\text{TiO}_x$  thicknesses being independent of the total film thickness. Fragmentation testing was employed to investigate the fracture behavior as well as the adhesion behavior by using the dimensions of the tensile-induced buckles which formed between crack fragments. Of note was a change in the crack path from straight to zig-zag as the film thickness was increased. The shear lag model was applied to determine the interfacial shear stress and found that the 12 nm film had the lowest value. This, along with the presence of both straight and zig-zag cracking, could be an indication of a critical film thickness or grain size for the activation of toughening mechanisms. Adhesion does not change with decreasing Ti thickness (average  $4.5 \text{ Jm}^{-2}$ ) and compares well to other metal–polymer systems. What this study brings forward is the fact that very small changes in the film microstructure or thickness could have dramatic effects on the mechanical behavior. Also, that the thinner Ti films were made of more than 50% of another material should be a concern. The common assumption that the interface is sharp and grain size is on the order of the film thickness does not necessarily hold true for metal films on

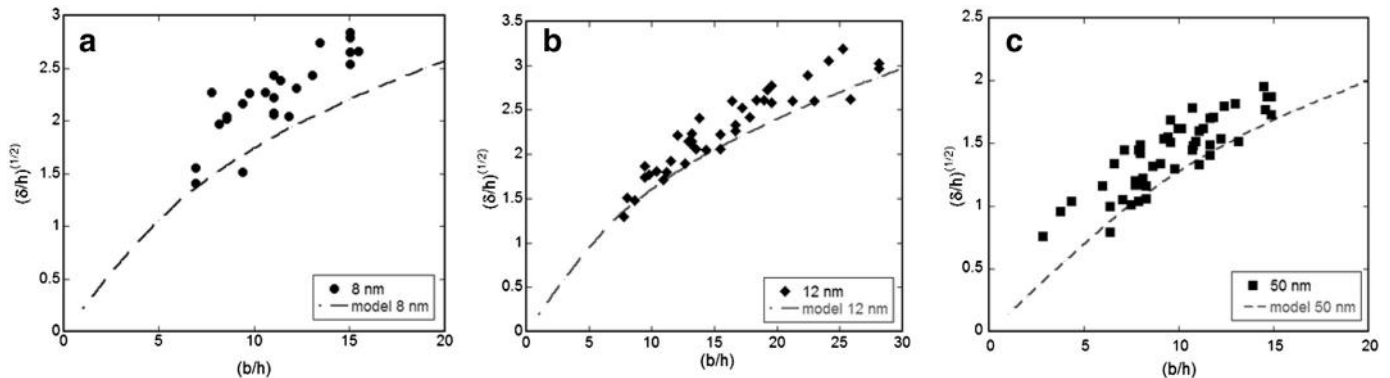


**Fig. 7.** The adhesion energies of the three Ti films were calculated by fitting the buckle data with Eq. (2) using a minimum  $\alpha_A$  value: (a) 8 nm, (b) 12 nm, and (c) 50 nm films. Each data point represents one buckle measurement.

polymers and these systems should be characterized more fully in order completely understand the mechanical behavior.

## Acknowledgments

AAT would like to thank B.G. Mendis for his support and advice during this work.

## References

- [1] G. Kettlgruber, M. Kaltenbrunner, C.M. Siket, R. Moser, I.M. Graz, R. Schwoediauer, S. Bauer, S. Bauer, Intrinsically stretchable and rechargeable batteries for self-powered stretchable electronics, *J. Mater. Chem. A* 1 (2013) 5505.
- [2] M.L. Hammock, A. Chortos, B.C.K. Tee, J.B.H. Tok, Z. Bao, 25<sup>th</sup> anniversary article: The evolution of electronic skin (E-Skin): a brief history, design considerations, and recent progress, *Adv. Mater.* 25 (2013) 5997.
- [3] D.C. Agrawal, R. Raj, Measurement of the ultimate shear strength of a metal–ceramic interface, *Acta Metall.* 37 (1998) 1265.
- [4] J. Andersons, S. Tarasovs, Y. Leterrier, Evaluation of thin film adhesion to a compliant substrate by the analysis of progressive buckling in the fragmentation test, *Thin Solid Films* 517 (2009) 2007.
- [5] S. Frank, U.A. Handge, S. Olliges, R. Spolenak, The relationship between thin film fragmentation and buckle formation: synchrotron-based in situ studies and two-dimensional stress analysis, *Acta Mater.* 57 (2009) 1442.
- [6] A.A. Taylor, M.J. Cordill, G. Dehm, On the limits of the interfacial yield model for fragmentation testing of brittle films on polymer substrates, *Philos. Mag.* 92 (2012) 3363.
- [7] M.J. Cordill, A. Taylor, J. Schalko, G. Dehm, Fracture and delamination of chromium thin films on polymer substrates, *Metall. Mater. Trans.* 41A (2010) 870.
- [8] O. Glushko, M.J. Cordill, Electrical resistance of metal films on polymer substrates under tension, *Exp. Tech.* 38 (2014) 1, <http://dx.doi.org/10.1111/ext.12082>.
- [9] N. Lu, Z. Suo, J.J. Vlassak, The effect of film thickness on the failure strain of polymer-supported metal films, *Acta Mater.* 58 (2010) 1679.
- [10] A. Kelly, W.R. Tyson, Tensile properties of fibre-reinforced metals: copper/tungsten and copper/molybdenum, *J. Mech. Phys. Solids* 13 (1965) 329.
- [11] A.A. Taylor, V. Edlmayr, M.J. Cordill, G. Dehm, The effect of film thickness variations in periodic cracking: analysis and experiment, *Surf. Coat. Technol.* 206 (2011) 1830.
- [12] M.J. Cordill, F.D. Fischer, F.G. Rammerstorfer, G. Dehm, Adhesion energies of Cr thin films on polyimide determined from buckling: experiment and model, *Acta Mater.* 58 (2010) 5520.
- [13] A.A. Taylor, M.J. Cordill, L. Bowles, J. Schalko, G. Dehm, An elevated temperature study of a Ti adhesion layer on polyimide, *Thin Solid Films* 531 (2013) 354.
- [14] M.J. Cordill, K. Schmidegg, G. Dehm, Interface failure and adhesion measured by focused ion beam cutting of metal–polymer interfaces, *Philos. Mag. Lett.* 91 (2011) 530.
- [15] M.J. Cordill, A.A. Taylor, J. Schalko, G. Dehm, Microstructure and adhesion of as-deposited and annealed Cu/Ti films on polyimide, *Int. J. Mater. Res.* 102 (2011) 729.
- [16] M.J. Cordill, V.M. Marx, C. Kirchlechner, Ductile film delamination from compliant substrates using hard overlayers, *Thin Solid Films* 571 (2014) 302.
- [17] V.M. Marx, C. Kirchlechner, I. Zizak, M.J. Cordill, G. Dehm, Adhesion measurement of a buried Cr interlayer on polyimide, *Philos. Mag.* (2014), <http://dx.doi.org/10.1080/14786435.2014.920543> in press.
- [18] K. Wu, J.Y. Zhang, G. Liu, P. Zhang, P.M. Cheng, J. Li, G.J. Zhang, J. Sun, Buckling behaviors and adhesion energy of nanostructured Cu/X (X = Nb, Zr) multilayer films on a compliant substrate, *Acta Mater.* 61 (2013) 7889.
- [19] Y. Leterrier, Y. Wyser, J.A.E. Manson, J. Hilborn, A method to measure the adhesion of thin glass coatings on polymer films, *J. Adhes.* 44 (1994) 213.
- [20] T. Li, Z.Y. Huang, Z.C. Xi, S.P. Lacour, S. Wagner, Z. Suo, Delocalizing strain in a thick metal film on a polymer substrate, *Mech. Mater.* 37 (2005) 261.
- [21] T. Li, Z. Suo, Deformability of thin metal films on elastomer substrates, *Int. J. Solids Struct.* 44 (2006) 1696.
- [22] A. Hohenwarter, C. Kammerhofer, R. Pippan, The ductile to brittle transition of ultrafine-grained Armco iron: an experimental study, *J. Mater. Sci.* 45 (2010) 4805.
- [23] A. Latapie, D. Farkas, Molecular dynamics investigation of the fracture behavior of nanocrystalline  $\alpha$ -Fe, *Phys. Rev. B* 69 (2004) (134110-1-9).
- [24] L.A. Giannuzzi, F.A. Stevie, Introduction to Focused Ion Beams: Instrumentation, Theory, Techniques and Practice, Springer Science & Business Media, Inc, New York, 2005.
- [25] A.A. Taylor, M.J. Cordill, G. Moser, G. Dehm, A mechanical method for preparing TEM samples from brittle films on compliant substrates, *Prakt. Metallogr.* 48 (2011) 408.
- [26] C.A. Schneider, W.S. Rasband, K.W. Eliceiri, NIH Image to ImageJ: 25 years of image analysis, *Nat. Methods* 9 (2012) 671.
- [27] I.S. Park, J. Yu, An x-ray study on the mechanical effects of the peel test in a Cu/Cr/polyimide system, *Acta Mater.* 46 (8) (1998) 2947.
- [28] Y. Nakamura, Y. Suzuki, Y. Watanabe, Effect of oxygen plasma etching on adhesion between polyimide films and metal, *Thin Solid Films* 290–291 (1996) 367.
- [29] N.J. Chou, C.H. Tang, Interfacial reaction during metallization of cured polyimide: an XPS study, *J. Vac. Sci. Technol. A* 2 (1984) 751.
- [30] N.J. Chou, D.W. Dong, J. Kim, A.C. Liu, An XPS and TEM study of intrinsic adhesion between polyimide and Cr films, *J. Electrochem. Soc.* 131 (10) (1984) 2335.
- [31] Y.H. Kim, J. Kim, G.F. Walker, C. Feger, S.P. Kowalczyk, Adhesion and interface investigation of polyimide on metals, *J. Adhes. Sci. Technol.* 2 (1988) 95.
- [32] P.S. Ho, P.O. Hahn, J.W. Bartha, G.W. Rubloff, F.K. LeGoues, Chemical bonding and reaction at metal/polymer interfaces, *J. Vac. Sci. Technol. A* 3 (1985) 739.
- [33] A.R. Rossi, P.N. Sanda, B.D. Silverman, P.S. Ho, A theoretical study of the bonding and XPS spectra of chromium interacting with a polyimide model compound, *Organometallics* 6 (1987) 580.
- [34] R.C. White, R. Haight, B.D. Silverman, P.S. Ho, Cr– and Cu–polyimide interface: chemistry and structure, *Appl. Phys. Lett.* 51 (1987) 481.
- [35] T.-G. Chung, Y.-H. Kim, J. Yu, An Auger study on the interactions of Cu and Cr films with polyimide, *J. Adhes. Sci. Technol.* 8 (1994) 41.
- [36] R. Saha, W.D. Nix, Effects of the substrate on the determination of thin film mechanical properties by nanoindentation, *Acta Mater.* 50 (2002) 23.
- [37] M.J. Barber, K.E. Cooke, A.B. Mann, B. Derby, Accurate determination of Young's modulus and Poisson's ratio of thin films by a combination of acoustic microscopy and nanoindentation, *Thin Solid Films* 398–399 (2001) 299.
- [38] W.D. Nix, Mechanical properties of thin films, *Metall. Trans. A* 20 (1989) 2217.
- [39] J. Chen, S.J. Bull, On the factors affecting the critical indenter penetration for measurement of coating hardness, *Vacuum* 83 (2009) 911.